Journal of the Mechanics and Physics of Solids 109 (2017) 22–33

Contents lists available at ScienceDirect

Journal of the Mechanics and Physics of Solids

journal homepage: www.elsevier.com/locate/jmps

Architected squirt-flow materials for energy dissipation

Tal Cohen[a,b,*], Patrick Kurzeja[c], Katia Bertoldi[d]

[a] Department of Civil & Environmental Engineering, Massachusetts Institute of Technology, 77 Massachusetts Avenue Cambridge, MA, 02139, USA
[b] Department of Mechanical Engineering, Massachusetts Institute of Technology, 77 Massachusetts Avenue Cambridge, MA, 02139, USA
[c] Institute of Mechanics, Technical University Dortmund, Leonhard-Euler-Str. 5, Dortmund, 44227, Germany
[d] John A. Paulson School of Engineering and Applied Sciences, Harvard University, 29 Oxford Street, Cambridge, MA, 02138, USA

ARTICLE INFO

Article history:
Received 15 March 2017
Revised 3 August 2017
Accepted 7 August 2017
Available online 8 August 2017

Keywords:
Reversible energy dissipation
Squirt-flow
Relaxation

ABSTRACT

In the present study we explore material architectures that lead to enhanced dissipation properties by taking advantage of squirt-flow - a local flow mechanism triggered by heterogeneities at the pore level. While squirt-flow is a known dominant source of dissipation and seismic attenuation in fluid saturated geological materials, we study its untapped potential to be incorporated in highly deformable elastic materials with embedded fluid-filled cavities for future engineering applications. An analytical investigation, that isolates the squirt-flow mechanism from other potential dissipation mechanisms and considers an idealized setting, predicts high theoretical levels of dissipation achievable by squirt-flow and establishes a set of guidelines for optimal dissipation design. Particular architectures are then investigated via numerical simulations showing that a careful design of the internal voids can lead to an increase of dissipation levels by an order of magnitude, compared with equivalent homogeneous void distributions. Therefore, we suggest squirt-flow as a promising mechanism to be incorporated in future architected materials to effectively and reversibly dissipate energy.

1. Introduction

From space crafts, cars and buildings to cell phones, tablets and micro-scale electric devices, the ability of a structure to both dissipate and mitigate energy upon impact and vibration is imperative to its functionality. Some engineered structures are equipped with dedicated devices, such as hydraulic pistons and rubber bearings, to damp unwanted vibrations or to absorb shocks. However, this strategy has some obvious shortcomings (such as the use of multiple components and the possible failure at the interfaces between them), thus motivating the search for materials that inherently dissipate mechanical energy.

It is well known that energy dissipation can be achieved by the frictional interaction between a solid and an impregnating fluid. For example, fluid saturated materials have been extensively studied to enhance energy dissipation and shock absorption in the context of protective armor for protection against explosive pressure gradients (Bettin and McKinley, 2005; Dawson, 2009; Dawson et al., 2008; 2009). A similar mechanism of dissipation is observed also in biological materials and explains, for example, *hydraulic stiffening* in bones (Zhang et al., 1998) and shock absorption in our muscles (Cohen and Givli,

* Corresponding author at: Department of Civil & Environmental Engineering, Massachusetts Institute of Technology, 77 Massachusetts Avenue Cambridge, MA, 02139, USA.
E-mail address: talco@mit.edu (T. Cohen).

http://dx.doi.org/10.1016/j.jmps.2017.08.003
0022-5096/

2014). In contrast to engineered fluid saturated systems that can employ different materials, but are usually designed to have a regular homogenous distribution of open celled voids that perform reversibly only at small strains; biological systems are limited in choice of materials and must be able to reversibly undergo large deformations. Therefore, they have evolved to achieve increased performance by correlating their internal hierarchial design with the experienced loading conditions and physical constraints (Fratzl et al., 2016). In that spirit, we attempt to establish herein a framework for incorporation of internal features in material components to achieve reversible energy dissipation and mitigation via a mechanism of solid-fluid interaction.

To address this challenge we adopt a particular mechanism of dissipation observed in natural systems known as *squirt-flow*[1] (Adelinet et al., 2011; Dvorkin and Nur, 1993; Gurevich et al., 2010; Müller et al., 2010; Quintal et al., 2011; Rubino et al., 2008). This phenomenon plays a dominant role in dissipation and attenuation of seismic waves in fluid saturated media and is due to the local flow of fluid between one cavity to another to relieve internal stresses that are generated by heterogeneities at the pore scale. As explained by Dvorkin and Nur (1993), conventional macroscopic models of poroelasticity fail to account for this dominant mechanism of dissipation, which is largely dependent upon the local pore geometry. Moreover, available models rarely account for the combination of large strains and the coupled fluid-solid interaction (Schraad and Harlow, 2006). Averaging methods neglect the effect of local heterogeneities and orthotropy on dissipation or compensate for their effect artificially by inserting empirical correction terms, with the underlying assumption that these effects are small (Comiti and Renaud, 1989). In the present study we ask whether that 'small' effect can be significantly enhanced by design. We consider a closed system comprised of an array of interconnected fluid-filled cavities embedded in a compressible hyperelastic medium. Hence, although squirt-flow is a dissipative process the initial stress free state is fully recovered once the load is relieved, without the need for any external assistance. It will be shown that an intelligently designed internal architecture that correlates with the expected loading conditions can increase the dissipation levels by an order of magnitude.

Measures for the effectiveness of a solid in energy dissipation are usually well defined only in the linear regime (Graesser and Wong, 1991). In the present study we are concerned with dissipation at large strains and thus we adopt the *dissipation efficiency* measure (Cohen et al., 2014; Cohen and Givli, 2014) which represents the fraction of energy dissipation with respect to the total energy input in a single relaxation test and reduces to the well known linear measures (i.e. the *inverse quality factor* or the *loss factor*) in the small-strains regime. This approach provides an absolute measure for the energy dissipation capability of the material without dependence on a specific loading rate or frequency. The systems considered in this study are made of hyperelastic materials and are subjected to large deformation. Most rubber-like materials that are capable of large deformations exhibit significant hysteresis and thus have an inherent capability to dissipate energy, with a dissipation efficiency of the order of $\sim 10\%$ (Gent, 2012). Therefore these materials are regularly used as damping components in engineering applications of various length scales from electric devices to bridges and sky-scrapers in earthquake prone regions (Gent, 2012). For the present investigation we decouple the intrinsic dissipation of the material and show that by integrating a squirt-flow mechanism into a rate-independent material one can potentially dissipate a significant percentage of the invested energy in a single relaxation response. To study the constitutive sensitivity of the dissipation efficiency, we consider materials of varying compressibility levels. Although rubber-like materials are only weakly compressible, high compressibility can be achieved by employing architected matrix materials, such as foams. Nonetheless, our results indicate that materials with practical compressibility levels are most efficient in squirt dissipation.

The paper is organized as follows: First, in Sections 2 and 3, we present an analytical investigation of an idealized squirt cell which accommodates both a compressible elastic solid and an incompressible fluid. We show that in idealized settings and under large deformations, squirt-flow can result in more than 50% energy dissipation, adding significantly to the inherent dissipation properties of the matrix material. Then, in Section 4 we proceed to consider a number of realizations of the idealized squirt cell, which are investigated via numerical simulation. Finally, in Section 5 we design architected materials with embedded squirt cells and show that their dissipation efficiency can be by an order of magnitude larger than that of equivalent homogeneous designs.

2. The idealized squirt cell

To derive a theoretical prediction of the dissipation levels achievable by squirt-flow and their sensitivity to model parameters, we begin by formulating an idealized model in which two deformable units are allowed to exchange fluids to relive stresses.

2.1. A single unit

We start by considering a single closed unit which accommodates both a compressible elastic solid and an incompressible fluid, say water, as illustrated in Fig. 1. We assume plane-strain conditions and organize the two materials so that in the undeformed configuration the solid occupies a rectangle of height h_0 and length l_0^s, and the water occupies a rectangle of height h_0 and length l_0^w. The constant out-of-plane thickness of the unit is w_0. It follows that the total initial length of the unit is $l_0 = l_0^s + l_0^w$ and that the volume fraction of water in the unit is $\phi_0 = l_0^w / l_0$.

[1] Note that, in the literature, squirt-flow is also referred to as local flow and pressure diffusion (Adelinet et al., 2011; Ciz et al., 2006).

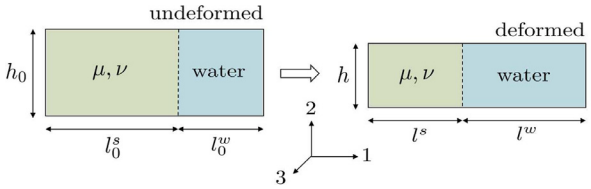

Fig. 1. A single unit in both undeformed (left) and deformed (right) configurations. The deformation is imposed by changing the unit height from h_0 to h, while keeping its length ($l_0 = l_0^s + l_0^w$) constant.

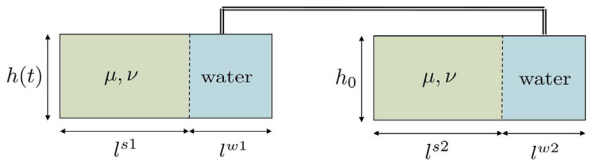

Fig. 2. The squirt cell: two units are attached to allow flow of water through a channel. The cell is deformed by changing the height of the left unit while the right unit remains at constant height.

We consider an idealized scenario in which the unit is deformed by changing only its height (to the deformed value h), while keeping its length constant (i.e. $l = l_0$). For simplicity, we assume that the two materials conserve a rectangular shape, so that the deformation within the solid is uniform and can be described by the principal stretches

$$\lambda_1 = \frac{l^s}{l_0^s}, \qquad \lambda_2 = \frac{h}{h_0}, \qquad \lambda_3 = 1. \tag{1}$$

Moreover, the requirement of conservation of fluid volume yields

$$\lambda_1 = \frac{\lambda_2 - \phi_0}{(1-\phi_0)\lambda_2}. \tag{2}$$

Considering a compressible neo-Hookean material, the elastic strain energy per unit of undeformed solid volume reads (Ogden, 1997)

$$\mathcal{E} = \frac{\mu}{3}\left[\frac{3}{2}\left(\frac{I}{J^{2/3}} - 3\right) + \beta(J-1)^2\right], \tag{3}$$

where $J = \lambda_1\lambda_2\lambda_3$ and $I = \lambda_1^2 + \lambda_2^2 + \lambda_3^2$. The principal Cauchy stress components are then obtained from (3) as

$$\sigma_i = \frac{\mu}{3}\left[\left(\frac{3\lambda_i^2 - I}{J^{5/3}}\right) + 2\beta(J-1)\right], \quad i = 1, 2, 3 \tag{4}$$

where μ is the initial shear modulus and

$$\beta = \frac{1+\nu}{1-2\nu}, \tag{5}$$

is a measure of the initial compressibility, with ν denoting the initial Poisson's ratio of the material. Note that any alternative constitutive model for compressible hyperelastic materials can be employed and is expected to yield similar qualitative behavior. For the current investigation, the neo-Hookean form was chosen since it conveniently reduces to represent linear elastic behavior with the regular elastic constants in the small-strains regime.

Finally, since the hydrostatic pressure in the fluid (p) must equilibrate the stress component in the direction normal to the interface with the solid, we have

$$p = \sigma_1 = \frac{\mu}{3}\left[\left(\frac{3\lambda_1^2 - I}{J^{5/3}}\right) + 2\beta(J-1)\right]. \tag{6}$$

2.2. The squirt cell

Now, since we are interested in squirt-flow, we can conceptually connect two such units by a channel which allows for flow of water from one unit to the other, as shown in Fig. 2. For the sake of simplicity, we take two initially identical units (unit '1' and unit '2'). We then apply a deformation to unit '1' by varying its height from h_0 to $h^{(1)}$, while keeping its length constant (i.e. $l^{(1)} = l_0$). At the same time we keep the dimensions of unit '2' constant (i.e. $V^{(2)}(t) = V_0 = w_0 h_0 l_0$). Fluid incompressibility implies that the total fluid volume in the system is also constant (i.e. $V^{w(1)}(t) + V^{w(2)}(t) = 2w_0 h_0 l_0^w$), so that we have a dynamic system with one control variable - $\lambda(t) = h^{(1)}/h_0$ - and one degree of freedom - $\phi(t) = h^{(1)} l^{w(1)}/(h_0 l_0)$ -

the fraction of fluid volume in unit '1'. Note that here and in the following all quantities with superscripted (1) and (2) refer to unit '1' and unit '2', respectively, while the system parameters $\lambda(t)$ and $\phi(t)$ refer to unit '1'. Given the fluid volume in the units and their height, we can write the stretch components as

$$\lambda_1^{(1)} = \frac{\lambda - \phi}{(1-\phi_0)\lambda}, \quad \lambda_2^{(1)} = \lambda = \frac{h^{(1)}}{h_0}, \quad \lambda_3^{(1)} = 1 \tag{7}$$

for unit '1', and

$$\lambda_1^{(2)} = 1 + \frac{\phi - \phi_0}{1-\phi_0}, \quad \lambda_2^{(2)} = 1, \quad \lambda_3^{(2)} = 1 \tag{8}$$

for unit '2'.

By introducing Eqs. (7) and (8) into Eq. (6) we obtain the fluid pressure $p^{(i)}$ in the two units as

$$p^{(1)} = \frac{2\mu}{3}\left[\lambda^{-2}\left(\frac{\lambda-\phi}{1-\phi_0}\right)^{-1/3} - \frac{1}{2}\left(\lambda^2+1\right)\left(\frac{\lambda-\phi}{1-\phi_0}\right)^{-5/3} + \beta\left(\frac{\lambda-1}{1-\phi_0} + \frac{\phi_0-\phi}{1-\phi_0}\right)\right], \tag{9}$$

and

$$p^{(2)} = \frac{2\mu}{3}\left[\left(1+\frac{\phi-\phi_0}{1-\phi_0}\right)^{-1/3} - \left(1+\frac{\phi-\phi_0}{1-\phi_0}\right)^{-5/3} + \beta\left(\frac{\phi-\phi_0}{1-\phi_0}\right)\right], \tag{10}$$

The rate of volume exchange between the two units can be estimated by Poiseuille's law

$$\frac{dV^{w(1)}}{dt} = \frac{\pi R^4 \Delta p}{8\tau L} \quad \text{with} \quad \Delta p = p^{(1)} - p^{(2)} \tag{11}$$

where τ is the fluid viscosity and L, R are the length and radius of the connecting pipe, respectively. By substituting Eqs. (9) and (10) into Eq. (11), we arrive at the first order, nonlinear differential equation

$$\begin{aligned}\gamma\frac{d\phi}{dt} = {} & \beta\left[\frac{\lambda-1}{1-\phi_0} + 2\left(\frac{\phi_0-\phi}{1-\phi_0}\right)\right] + \lambda^{-2}\left(\frac{\lambda-\phi}{1-\phi_0}\right)^{-1/3} - \left(1+\frac{\phi-\phi_0}{1-\phi_0}\right)^{-1/3} \\ & + \left(1+\frac{\phi-\phi_0}{1-\phi_0}\right)^{-5/3} - \frac{1}{2}\left(\lambda^2+1\right)\left(\frac{\lambda-\phi}{1-\phi_0}\right)^{-5/3},\end{aligned} \tag{12}$$

where

$$\gamma = \frac{12 h_0 l_0 w_0 L \tau}{\pi R^4 \mu}. \tag{13}$$

defines the time-scale of the squirt system and thus dictates the regime of application of Poiseuille's law. More specifically, both the flow rate and the Reynolds number scale with $1/\gamma$. Hence, to facilitate Poiseuille's flow, the model parameters entering in (13) can be adjusted to maximize γ. However, it is also important to note that, if the limits of Poiseuille's flow are exceeded and the flow becomes turbulent, the present study provides a lower bound estimation of the achieved dissipation.

Finally, we note that, since the system arrives at equilibrium once $d\phi/dt \to 0$, the equilibrium volume ratio of unit '1' (ϕ_∞) can be obtained by solving the implicit relation

$$\begin{aligned}& \beta\left[\frac{\lambda-1}{1-\phi_0} + 2\left(\frac{\phi_0-\phi}{1-\phi_0}\right)\right] + \lambda^{-2}\left(\frac{\lambda-\phi}{1-\phi_0}\right)^{-1/3} - \left(1+\frac{\phi-\phi_0}{1-\phi_0}\right)^{-1/3} \\ & + \left(1+\frac{\phi-\phi_0}{1-\phi_0}\right)^{-5/3} - \frac{1}{2}\left(\lambda^2+1\right)\left(\frac{\lambda-\phi}{1-\phi_0}\right)^{-5/3} = 0.\end{aligned} \tag{14}$$

3. Energy dissipation

Although several measures for the effectiveness of a material in dissipating energy are available in the literature, they are usually well defined only in the linear regime (Graesser and Wong, 1991). Since in the present study we are concerned with dissipation at large strains, we assess the dissipation response by considering the percentage of energy dissipation with respect to the total energy input in a relaxation test. We refer to this quantity as the *dissipation efficiency* (η) and obtain it as the ratio between the dissipated energy (E_d) and the total energy invested in the system (E_t)

$$\eta = \frac{E_d}{E_t} = 1 - \frac{E_e}{E_t}, \tag{15}$$

where E_e is the elastic energy stored in the system (i.e. $E_e = E_t - E_d$). Note that in the linear limit η corresponds to the *inverse quality factor* or *loss factor* (Graesser and Wong, 1991). For the idealized squirt cell the elastic energy (per unit volume) stored in the system is obtained by inserting Eqs. (7) and (8) into Eq. (3) and accounting for both units, which yields

$$E_e = \frac{(1-\phi_0)\mu}{3}\left[\frac{3}{2}\left(\frac{I^{(1)}}{(J^{(1)})^{2/3}} + \frac{I^{(2)}}{(J^{(1)})^{2/3}} - 6\right) + \beta\left((J^{(1)}-1)^2 + (J^{(2)}-1)^2\right)\right] \tag{16}$$

In this study, to obtain an absolute measure for the efficiency of the considered systems in dissipating energy, which does not depend on a specific loading rate or frequency and applies also in the nonlinear regime, we subject the structure to an instantaneous deformation

$$\lambda(t) = \lambda_0 \mathcal{H}(t), \tag{17}$$

with $\mathcal{H}(t)$ denoting the Heaviside function. Then, we hold the structure in strained condition until the fluid arrives at equilibrium. Note that for such loading conditions no additional external work is done throughout the relaxation time. Therefore the total dissipation (E_d) can be calculated as the difference between the initial and final elastic energy (E_e) and the dissipation efficiency (15) reads

$$\eta = 1 - \frac{E_e(t=\infty)}{E_e(t=0^+)}. \tag{18}$$

Now, to characterize the ability of the squirt cell described in Section 2.2 to dissipate energy, we apply to unit '1' the instantaneous deformation (17) with the initial condition

$$\phi(t=0) = \phi_0 \tag{19}$$

and keep the volume of unit '2' constant. The dissipation efficiency η can then be calculated using Eq. (18). The initial elastic energy (i.e. $E_e(t=0^+)$) is obtained by inserting $\lambda = \lambda_0$ and $\phi = \phi_0$ in Eq. (16). On the other hand, the final amount of elastic energy stored in the system (i.e. $E_e(t=\infty)$) is found from Eq. (16) by substituting $\lambda = \lambda_0$ and $\phi = \phi_\infty$, as given by solving Eq. (14).

3.1. Small-strains dissipation efficiency

While for nonlinear finite deformations the dissipation efficiency can only be obtained numerically (since Eq. (18) depends on the implicit relation (14)) a closed form expression for η can be obtained when considering small-strains. Hence, to get further insight into the response of the system we first investigate the limit of small disturbances and consider scenarios for which both the strain

$$\epsilon(t) = \lambda(t) - 1, \tag{20}$$

and the volume exchange

$$\delta\phi(t) = \phi(t) - \phi_0, \tag{21}$$

are small (i.e. $\epsilon \ll 1$ and $\delta\phi \ll 1$). For such conditions Eq. (12) can be linearized, yielding

$$a\frac{d\delta\phi}{dt} + b\delta\phi = \epsilon(t) \tag{22}$$

with

$$a = \frac{(1-\phi_0)\gamma}{3\phi_0 + \beta - 1}, \quad \text{and} \quad b = \frac{2+4\beta}{3\phi_0 + \beta - 1}. \tag{23}$$

Solving Eq. (22) with the initial condition (19) and with the boundary condition (17) rewritten in terms of strain as $\epsilon(t) = \epsilon_0\mathcal{H}(t)$, results in the time dependant volume exchange

$$\delta\phi = \frac{\epsilon_0}{b}\left(1 - e^{-\frac{b}{a}t}\right), \tag{24}$$

indicating that the equilibrium configuration is reached when $\delta\phi \to \epsilon_0/b$.

Having determined the evolution of the fluid volume exchange, we can then evaluate the equivalent force (per unit length) applied to the squirt cell, which in the linear regime can be written as

$$f = \phi_0\sigma_1^{(1)} + (1-\phi_0)\sigma_2^{(1)}. \tag{25}$$

By substituting into this equation the stress components (4) (with the stretches and fluid volume exchange defined by Eqs. (7), (8) and (24)) and retaining only the linear order term, we obtain

$$f = \left(k_1 + k_2 e^{-\frac{b}{a}t}\right)\epsilon_0, \tag{26}$$

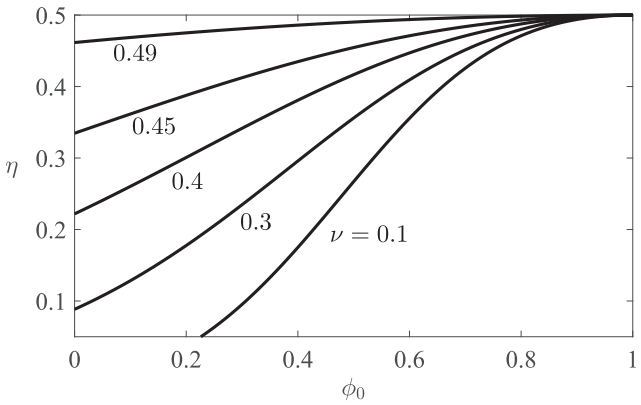

Fig. 3. Variation of the small-strains dissipation efficiency (Eq. (29)) as a function of the fluid volume fraction ϕ_0 for different values of the initial Poisson's ratio ν.

where

$$k_1 = \mu\left(\frac{(8\beta+1)\phi_0^2 - 2(5\beta+1)\phi_0 + \beta^2 + 4\beta + 1}{(1+2\beta)(1-\phi_0)}\right) \quad \text{and} \quad k_2 = \frac{2\mu}{b}\left(\frac{3\phi_0+\beta-1}{1-\phi_0}\right). \tag{27}$$

Interestingly, Eq. (26) reveals that the response of our squirt cell is identical to that of a *standard linearly viscoelastic material* (Lakes, 1998), which is represented by a combination of linear springs (with coefficients k_1 and k_2) and a dashpot (with damping coefficient $k_2(a/b)$). Although macroscopic models of fluid-saturated geological materials account for a number of different characteristic dissipation mechanisms and incorporate a number of different characteristic relaxation times (Renner and Steeb, 2014), in the linear limit the separate local contribution of a squirt cell can be simplified to the response of a standard linearly viscoelastic material (Carcione, 1998). Our focus on a simplified squirt cell can thus provide insights into the local squirt-flow response in fluid-saturated geological materials.

Next, by Taylor expanding Eq. (16) about $\epsilon = 0$ and $\delta\phi = 0$ and retaining terms up to the quadratic order, we obtain

$$E_e(\epsilon, \delta\phi) = \frac{\mu}{3}\left(\frac{\beta - 6(1-\phi_0)\phi_0 + 2}{1-\phi_0}\epsilon^2 - \frac{2(3\phi_0+\beta-1)}{1-\phi_0}\epsilon\delta\phi + \frac{2\beta+4}{1-\phi_0}\delta\phi^2\right), \tag{28}$$

so that the dissipation efficiency (18) can be written as

$$\eta = 1 - \frac{E_e(\epsilon_0, \epsilon_0/b)}{E_e(\epsilon_0, 0)} = \frac{(3\phi_0+\beta-1)2b - (2\beta+4)}{(6\phi_0(\phi_0-1) + (\beta+2))b^2}. \tag{29}$$

which, as expected in the linear regime, is independent of the applied strain (ϵ_0).

The asymptotic limits of the dissipation efficiency given in (29) can be examined by inserting limiting values of ϕ_0 and ν. Upon approaching incompressibility $\nu \to 1/2$ the dissipation efficiency tends to $\eta \to 1/2$, which is independent of the initial volume ratio. If the cell volume is dominated by fluid, with $\phi_0 \to 1$, then the dissipation efficiency approaches the same asymptotic limit of $\eta \to 1/2$, which is now independent of the material compressibility. This behavior is immediately noticeable in Fig. 3, where we present the small-strains dissipation efficiency as a function of the initial fluid volume ratio (ϕ_0) for different values of ν. The curves clearly indicate that the asymptotic value of $\eta = 1/2$ represents an upper bound in the linear regime, for which the dissipated energy equals the elastically stored energy. Additionally, we find that, as the volume fraction ϕ_0 decreases, the dissipation efficiency becomes highly sensitive to the initial material compressibility and quickly deteriorate as ν decreases.

3.2. Finite-strains dissipation efficiency

Next, we extend the analysis to account for finite strains and nonlinear effects and use Eqs. (16) and (18) to calculate the dissipation efficiency. In Fig. 4 we report the variation of η as a function of the instantaneous applied stretch λ_0 for different values of fluid volume fractions ϕ_0 (Fig. 4(a)) and different values of the initial Poisson's ratio ν (Fig. 4(b)). On both plots it is immediately noticeable that by applying compressive finite deformations, we are able to exceed the linear dissipation limit and achieve very high dissipation levels, well over $\eta = 1/2$. Interestingly, this dramatic sensitivity to nonlinear effects is observed only under compression (i.e. $\lambda_0 < 1$), while in tension the behavior is nearly passive to the nonlinearity. We also find that varying the initial volume fraction has a considerable effect on η. For $\phi_0 > 1/2$ a significant amount of energy is dissipated even when a small compressive deformation is applied to unit '1'. Finally, our results indicate that η is highly sensitive to the initial material compressibility and that at $\lambda_0 \sim 0.64$ an inversion of the curves occurs. This inversion, which is a result of nonlinear variations in the Poisson's effect (and depends on ϕ_0), suggests that the range of deformations in which a damping material is expected to perform should influence its design.

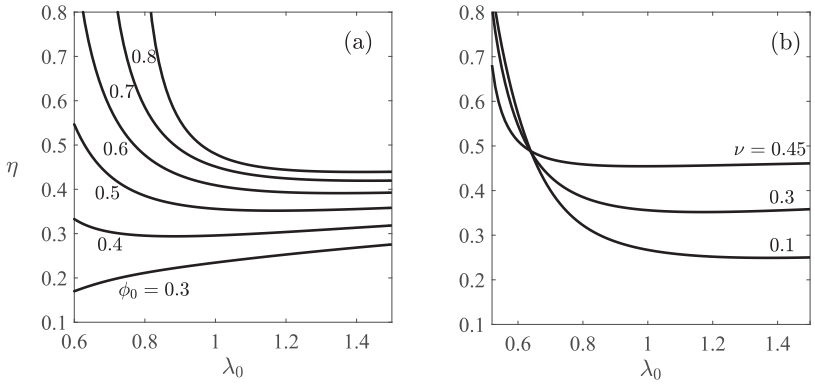

Fig. 4. Variation of the dissipation efficiency η as a function of the instantaneous applied stretch λ_0 (a) for different values of fluid volume fractions ϕ_0 (assuming $\nu = 0.3$) and (b) for different values of the initial Poisson's ratio ν (assuming $\phi_0 = 0.5$).

Although the results and conclusions derived here are limited to the specific setting and loading conditions of the considered idealized squirt cell, they provide useful guidelines for the design of efficient energy dissipating materials. In particular, they indicate that: (*i*) designing dissipation materials to perform in the nonlinear regime may have a significant effect on the achievable dissipation levels; (*ii*) the specific loading conditions (compression/tension), material properties, and fluid volume fraction, all play a significant role in defining the dissipation capabilities and should be tuned accordingly; and (*iii*) even in the linear regime, squirt-flow can allow for up to 50% energy dissipation. With these guidelines in mind, we now proceed to design realistic architected materials that exploit the squirt-flow mechanism to effectively dissipate energy.

4. Realization of the idealized squirt cell

In the previous section we have demonstrated that in an idealized setting the squirt-flow mechanism can generate significant energy dissipation. To investigate the possibility of achieving such high dissipation levels in a realistic setting, we now use Finite Element (FE) simulations and explore the response of more practical designs of the squirt cell. Our numerical analyses are conducted using the commercial package Abaqus/Standard 6.16 (Dassault Systems) and all our models are meshed using quadratic plane-strain triangular elements (Abaqus element type: CPE6H) with edge size $\sim 1/10$ of the smallest feature dimension. Moreover, the response of the solid material is captured using the compressible neo-Hookean model, as in Eq. (4), and surface-based fluid-filled cavities are introduced to model the interactions between the structure and the contained fluid. The fluid is considered to be incompressible and the cavities are interconnected by applying the fluid exchange capability with a linear dependence between volumetric flow rate and pressure difference, as in Eq. (11). Since the initial and final configurations and the overall energy dissipation in the relaxation scenario are not influenced by the specific rate of leakage and characteristics of the connections, those properties are chosen to achieve efficient computation times. However, it is important to note that the specific dimensions of the connecting pipes affect the Reynolds number and, therefore, the type of flow that develops. Finally, we note that the channels connecting the cavities are assumed to be external to the plane of the structure (so that they do not interfere with the deformation) and are indicated by straight lines in Figs. 5-9. Note that specific realizations of squirt-flow may not be able to fully decouple the interference between the connecting pipes and the deformation, nonetheless this effect can be minimized by design and is thus neglected herein. The response of the structures is then simulated conducting dynamic implicit simulations (*DYNAMIC module in Abaqus). Prescribed displacements are instantaneously applied to portions of the boundary at $t = 0$ and kept constant during the analysis. Note that the maximum applied strain levels considered in the numerical simulation is dictated by the possible closure of the cavities, since we do not account for self-contact in our analyses. The simulations are stopped when the structure reaches equilibrium and there is no more fluid exchange between connected cavities. Finally, the energy dissipation capability of the systems is characterized by extracting the total elastic strain energy (output variable ALLSE in Abaqus) immediately after the load is applied (i.e. at $t = 0^+$) and at the end of the simulations, and calculating the dissipation efficiency η according to Eq. (18).

4.1. Design (a)

We begin by conducting a systematic investigation of a model that closely resembles our idealized squirt cell. As shown in Fig. 5, design (a) comprises two units that are almost completely decoupled and mostly interact via the exchange of fluid between the two circular fluid filled cavities. Moreover, to mimic the loading conditions considered in our analytical exploration, the external faces of the structure are constrained to slide along the adjacent rigid walls, and the top face of the left unit is displaced in vertical direction to deform the cell. Snapshots of a representative structure at $t = 0^+$ (i.e. immediately after the deformation is applied) and at $t = \infty$ (i.e. when the fluid exchange between the two cavities ends) show that, as expected, at $t = 0^+$ the deformation is confined to the unit that has been loaded, while at $t = \infty$ both units are deformed.

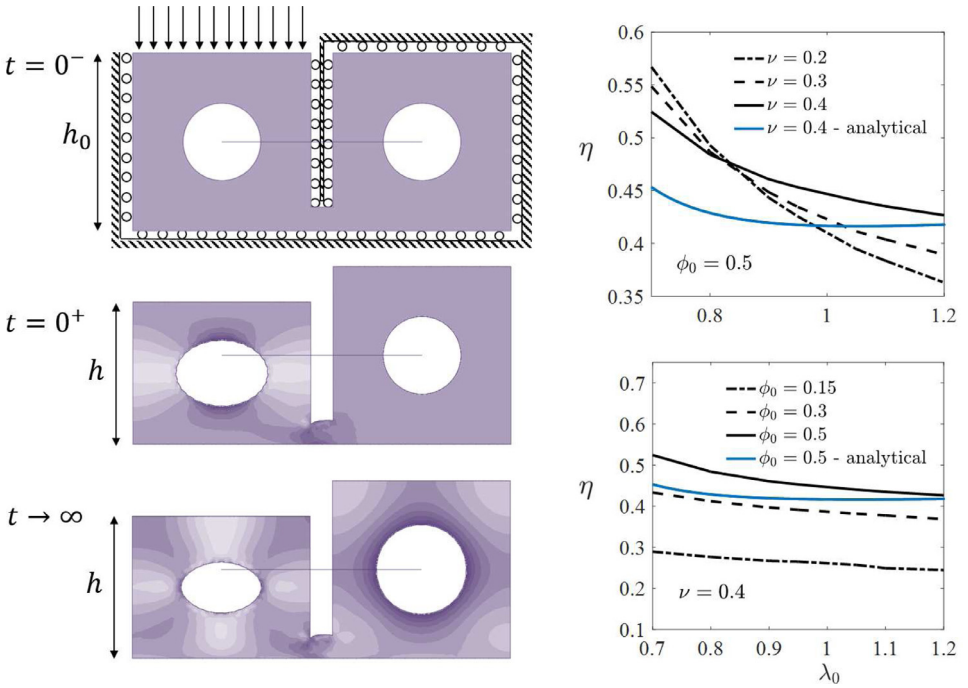

Fig. 5. Design (a): On the left - relaxation response of a representative squirt cell characterized by $\phi_0 = 0.15$ and $\nu = 0.4$ and subjected to $\lambda_0 = 0.8$. Numerical snapshots at $t = 0^-$ (stress free state), $t = 0^+$ (instantaneous purely elastic response) and $t \to \infty$ (relaxed state) are shown. The boundary conditions are shown in the stress free state. The applied stretch is calculated as $\lambda_0 = h/h_0$. The contours represent the maximum in-plane principle strain with the darker colors indicating tension and the brighter ones compression. The horizontal lines represent the connection between the cavities, thus allowing exchange of fluid. On the right - dissipation efficiency as a function of the applied stretch for different levels of ν (on the top) and ϕ_0 (on the bottom). The analytical prediction (Eq. (29)) for $\nu = 0.4$ and $\phi_0 = 0.5$ is shown in blue for comparison. (For interpretation of the references to color in this figure legend, the reader is referred to the web version of this article.)

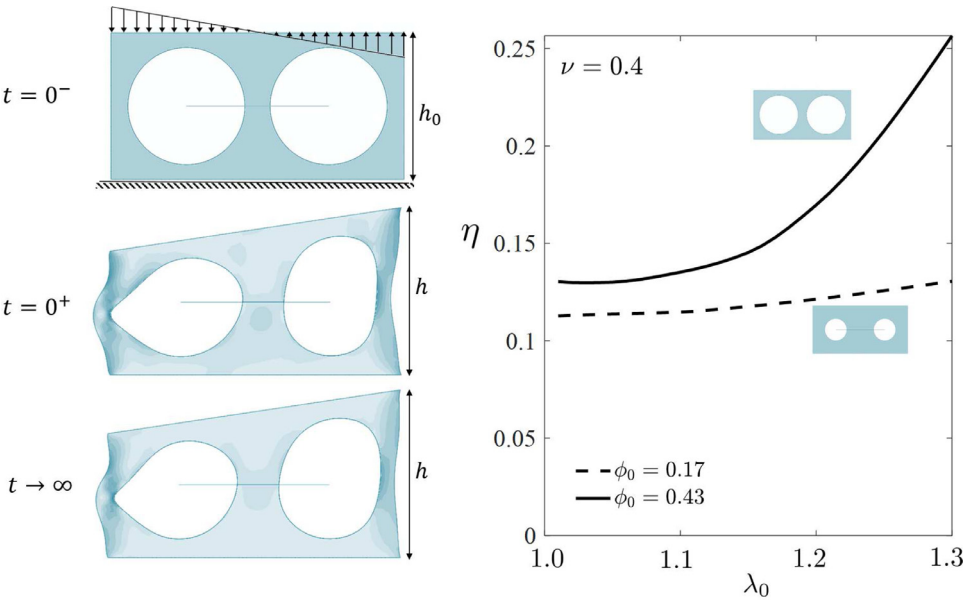

Fig. 6. Design (b): On the left - relaxation response of a representative squirt cell characterized by $\phi_0 = 0.43$ and $\nu = 0.4$ and subjected to $\lambda_0 = 1.25$. Numerical snapshots at $t = 0^-$ (stress free state), $t = 0^+$ (instantaneous purely elastic response) and $t \to \infty$ (relaxed state) are shown. The boundary conditions are shown in the stress free state. The applied stretch is calculated as $\lambda_0 = h/h_0$. The contours represent the maximum in-plane principle strain with the darker colors indicating tension and the brighter ones compression. The horizontal lines represent the connection between the cavities, thus allowing exchange of fluid. On the right - dissipation efficiency as a function of the applied stretch for different levels of ϕ_0 and with $\nu = 0.4$.

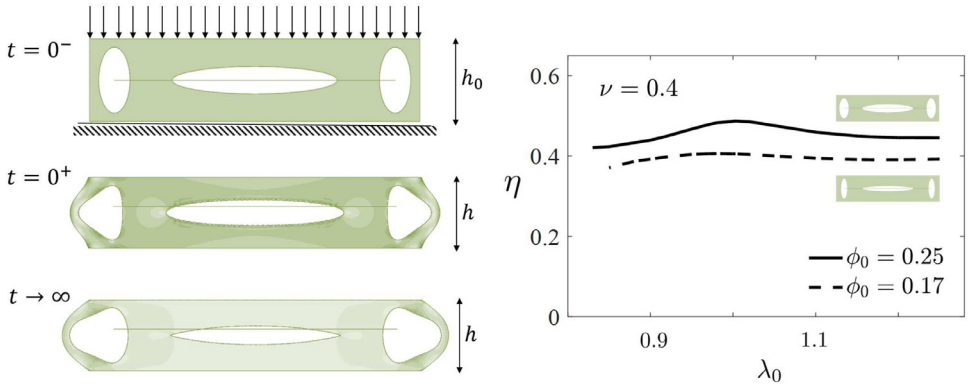

Fig. 7. Design (c): On the left - relaxation response of representative squirt cell with $\phi_0 = 0.25$ and $\nu = 0.4$ subjected to $\lambda_0 = 0.85$. Numerical snapshots at $t = 0^-$ (stress free state), $t = 0^+$ (instantaneous purely elastic response) and $t \to \infty$ (relaxed state) are shown. The boundary conditions are shown in the stress free state. The applied stretch is calculated as $\lambda_0 = h/h_0$. The contours represent the maximum in-plane principle strain with the darker shades for tension and brighter shades for compression. The horizontal lines represent the connection between the cavities, thus allowing exchange of fluid. On the right - dissipation efficiency as a function of stretch for different levels of ϕ_0 and with $\nu = 0.4$.

For this specific design and loading conditions (i.e. $\phi_0 = 0.15$, $\nu = 0.4$ and $\lambda_0 = 0.8$) the dissipation efficiency is $\eta \cong 0.28$. We further explore the effect of material compressibility and fluid volume fraction on η by changing ν and ϕ_0 (by equally varying the cavity radii). On the right-hand-side of Fig. 5 we report the evolution of the dissipation efficiency as a function of the applied stretch λ_0 for three different initial volume fractions (ϕ_0) and three different initial compressibility levels (ν). In the plots we also show the analytical predictions for the idealized squirt cell (blue lines) with $\phi_0 = 0.5$ and $\nu = 0.4$. The comparison between the analytical and numerical results indicate that the general trends found for the idealized squirt cell are maintained for design (a). In particular, a significant increase in dissipation, which can exceed the linear limit of $\eta = 1/2$, is observed in the large strains regime along with the inversion between curves in compression for different levels of ν. Finally, we note that the differences between analytical and numerical results are due to the significant distortions of the unit that are imposed in the idealized setting compared to the realized one.

4.2. Design (b)

The results shown in Fig. 5 indicate that design (a) is very efficient in dissipating energy and that its response closely resembles that of our idealized squirt cell. However, such a design is questionable from a practical point of view, since it requires to introduce an internal boundary between the two fluid filled cavities and to highly confine the edges of the structure. Therefore, we now investigate how η is affected by more realistic geometries and loading conditions. To this end, we introduce design (b), which comprises a rectangular block of solid material with two embedded identical and circular fluid filled cavities. As shown in Fig. 6, the bottom surface of the cell is fully constrained, the two side edges are traction free and deformation is applied by pushing on the top surface. Since for symmetric loading no fluid transfer is necessary to equilibrate the cell, design (b) can dissipate energy only if subjected to non-symmetric disturbances. Therefore, we apply the antisymmetric displacement distribution shown in Fig. 6, with maximum absolute applied displacement $h - h_0 = h_0(\lambda_0 - 1)$ as indicated in the figure. Guided by the results of the previous sections, we choose $\nu = 0.4$ to maximize the dissipation efficiency, while keeping a realistic level of material compressibility. In Fig. 6 we report the dissipation efficiency of design (b) for $\phi_0 = 0.17$ and 0.43 as a function of the amount of applied deformation. As for design (a), we find that η increases in the nonlinear regime. However, even for a high initial fluid volume fraction and large values of applied deformation, the dissipation efficiency does not exceed 25%. This is explained by the fact that, even for very large applied displacements, the fluid volume transfer between the two cavities is minimal.

4.3. Design (c)

To further improve the ability of the structure to dissipate energy, we consider a third design (design (c) - see Fig. 7) comprising three elliptical fluid filled cavities that are all connected to obtain dissipation under both symmetric and anti-symmetric loading conditions. As for design (b), the bottom surface of the cell is fully constrained, the two side edges are traction free and deformation is applied by pushing on the top surface. Note that this design is inspired by representative geometries reported for squirt-flow in geological materials (Rubino et al., 2008; Vinci et al., 2014). The alignment of the cavities and their locations are chosen to comply with the expected loading direction, while their dimensions are adjusted to vary the fluid volume ratio of the cell. Since the antisymmetric response of design (c) is qualitatively no different from that of design (b), here we focus on the symmetric response and apply an uniform displacement to the top surface.

In Fig. 7, we present results for $\phi_0 = 0.17$ and 0.25 with $\nu = 0.4$. We find that, differently from our previous designs, the behavior of this system is nearly passive to the nonlinearity both in tension and in compression. Essentially, design (c), by

accommodating the preferred mode of deformation under the given straining conditions (i.e. by taking advantage of the free edges and allowing material to migrate along the horizontal direction), is able to produce significant dissipation ($\eta > 0.42$) in the entire range. The high levels of dissipation in design (c) are maintained as long as there is fluid available to transfer from the central cavity to the exterior ones and vise versa, thus explaining the insensitivity of the dissipation efficiency to the increasing strain levels. As such, we expect the dissipation efficiency to deteriorate only when the cavities begin to close (since this will stop the flow). Thus further implying that the void volumes must be designed with regard to the expected level of applied deformation.

5. Realization of architected squirt-flow materials

Guided by our analytical investigation and numerical results, we proceed to design an architected material that optimally exploits squirt-flow to dissipate energy upon indentation. For the sake of simplicity, we focus on a rectangular block of material. The bottom surface of the block is fully constrained to a rigid substrate while its side faces are free. We consider two loading scenarios: a parabolic vertical deflection of the top surface, such that the two corners remain fixed and the mid-point experiences maximum displacement; and a uniform compressive deflection of the top surface, as shown on Figs. 8 and 9, respectively. For comparison we consider three designs that are shown, along with a representative relaxation response, in Figs. 8 and 9. Design (i) is a trivial design in which circular holes are distributed homogenously on a square grid. Though squirt-flow effects are possible in this setting, due to inhomogeneity in the loading conditions, this design should provide best agreement with available poroelasticity models (that are based on homogenized microstructures), especially as the

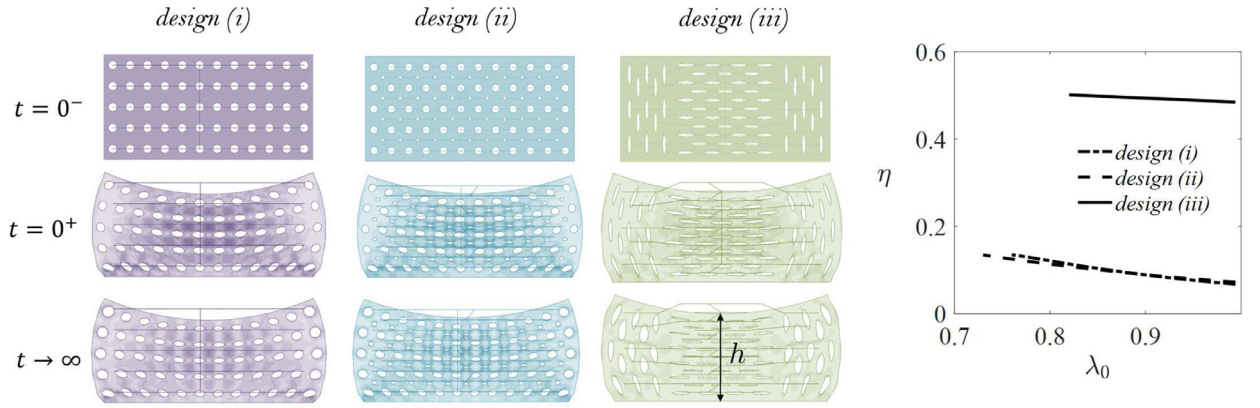

Fig. 8. Parabolic deflection of the top surface. On the left - relaxation response of representative architected materials with $\phi_0 = 0.17$ and $\nu = 0.4$ subjected to $\lambda_0 = h/h_0 = 0.82$ with h defined as the deformed hight of the midsection. Numerical snapshots at $t = 0^-$ (stress free state), $t = 0^+$ (instantaneous purely elastic response) and $t \to \infty$ (relaxed state) are shown. The contours represent the maximum in-plane principle strain with the darker shades for tension and brighter shades for compression. The lines represent the connection between the cavities, thus allowing exchange of fluid. On the right - dissipation efficiency as a function of applied stretch for the three designs.

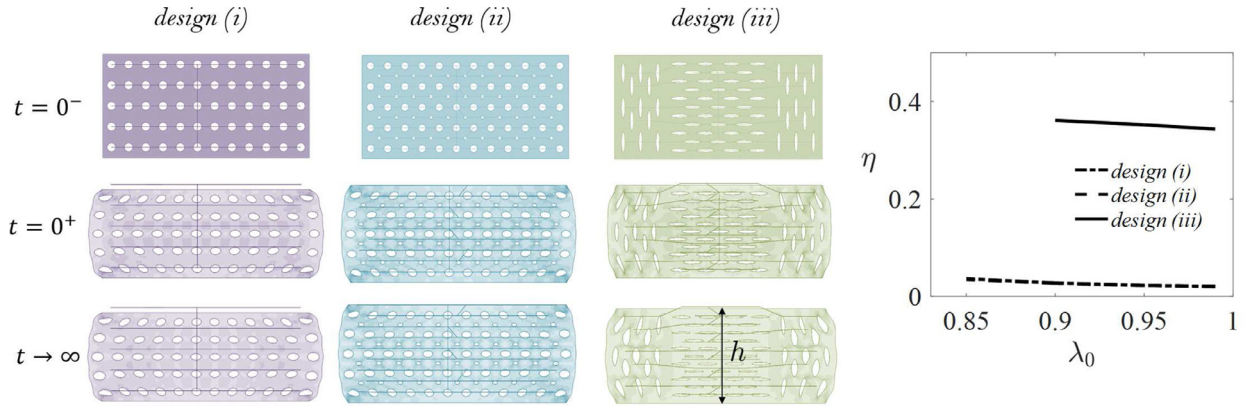

Fig. 9. Uniform compressive deflection of the top surface. On the left - relaxation response of representative architected materials with $\phi_0 = 0.17$ and $\nu = 0.4$ subjected to $\lambda_0 = h/h_0 = 0.9$. Numerical snapshots at $t = 0^-$ (stress free state and applied boundary conditions), $t = 0^+$ (instantaneous purely elastic response) and $t \to \infty$ (relaxed state) are shown. Numerical snapshots at $t = 0^-$ (stress free state), $t = 0^+$ (instantaneous purely elastic response) and $t \to \infty$ (relaxed state) are shown. The contours represent the maximum in-plane principle strain with the darker shades for tension and brighter shades for compression. The lines represent the connection between the cavities, thus allowing exchange of fluid. On the right - dissipation efficiency as a function of applied stretch for the three designs. Note that the results of designs (i) and (ii) virtually overlap.

cavities become smaller with respect to the dimensions of the component. In design (ii) all pores are still circular but with two different sizes, resulting in a hierarchical configuration which resembles the microstructure of double-porosity materials (Pride et al., 2003). Design (iii) is a squirt optimized design based on design (c) of the previous section. All three designs have an identical fluid volume fraction of $\phi_0 = 0.17$ and are made of a compressible neo-Hookean material with $\nu = 0.4$, so that the results for the dissipation efficiency are comparable. As understood from the previous sections, increasing the fluid volume fraction will increase the dissipation efficiency, however this sensitivity is not further investigated here. Finally, to allow for maximal relaxation, the connectivity between the cavities in all three designs is defined such that fluid from any one cavity can find a path to any other cavity.

Results for the dissipation efficiency of all three designs, under both loading scenarios, are shown on Figs. 8 and 9 and clearly reveal the advantage of the optimized squirt-flow architecture over the other designs. In both loading scenarios, the squirt-flow design exhibits dissipation efficiency levels that are higher by an order of magnitude and maintains the high efficiency throughout the entire range of applied stretch levels. In contrast to the response of a single squirt-cell, dissipation levels for the macroscopic design (design (iii)) increase monotonically with increasing strains and for large strains exceed the linear barrier of $\eta = 1/2$. This is attributed to the increasing participation of cells as the deformation levels increase. We also note that the responses of design (i) and design (ii) are almost identical, suggesting that hierarchial designs do not have a significant influence on dissipation levels. However, advantages of a hierarchial design may be in achieving increased fluid volume ratios or possibly in reducing stress levels. Nevertheless, these features of a hierarchial design are beyond the scope of the present study and should be subject for future investigations. Finally, the present results reveal a dramatic sensitivity of dissipation properties to the internal design of fluid filled features and indicate that squirt architected materials are promising candidates to enhance inherent dissipation properties in engineered damping components.

6. Concluding remarks

In this study we have combined analytical and numerical tools to investigate how squirt-flow influences the dissipation properties of highly deformable structures with embedded fluid-filled cavities. Our results indicate that dissipation levels can be increased by an order of magnitude by properly designing the architecture of the fluid saturated materials to enhance the squirt-flow mechanism. Hence, architected squirt-flow materials hold promise for future practical application as an internal damping mechanism in soft and compliant systems, such as soft robotic grippers, prosthetic joint implants and flexible electronics, as well as in damage mitigation of impact prone components, such as bumpers and landing gear. Moreover, since the optimal squirt design exhibits high levels of dissipation in the entire regime of applied strain levels, an additional avenue for future investigation of architected squirt-flow materials is in attenuation of pressure waves, with possible future application for acoustic isolation or even shock absorbtion. We note that the presented results do not take into consideration the intrinsic dissipation of the material and thus suggest a lower bound to the actual levels of dissipation. Moreover, an additional factor that has not been taken into consideration is the effect of temperature increase induced by the high levels of dissipation. Finally, although the extension of topology optimization algorithms to highly non-linear problems still remains unresolved, the insights gained through this study can be utilized in the future to guide the optimal design of fluid-saturated structures with desired dissipation properties and to possibly extend the analysis to account for more complex three dimensional geometries.

Acknowledgments

PK gratefully acknowledges support from German Research Foundation (Deutsche Forschungsgemeinschaft) grants KU 3351/1-1 and KU 3351/2-1. KB acknowledges support from NSF grant DMREF-1533985.

References

Adelinet, M., Fortin, J., Guéguen, Y., 2011. Dispersion of elastic moduli in a porous-cracked rock: theoretical predictions for squirt-flow. Tectonophysics 503 (1), 173–181.
Bettin, G., McKinley, G., 2005. High deformation rate behavior of polymeric foams filled with concentrated silica suspensions. The Society of Rheology 77th Annual Meeting.
Carcione, J.M., 1998. Viscoelastic effective rheologies for modelling wave propagation in porous media. Geophysical Prospecting 46 (3), 249–270.
Ciz, R., Saenger, E.H., Gurevich, B., 2006. Pore scale numerical modeling of elastic wave dispersion and attenuation in periodic systems of alternating solid and viscous fluid layers. J. Acoust. Soc. Am. 120 (2), 642–648.
Cohen, T., Durban, D., Society, T.R., 2014. Longitudinal shock waves in solids: the piston shock analogue. In: Proc. R. Soc. A. Vol. 470, p. 20130061.
Cohen, T., Givli, S., 2014. Dynamics of a discrete chain of bi-stable elements: a biomimetic shock absorbing mechanism. J. Mech. Phys. Solids 64, 426–439.
Comiti, J., Renaud, M., 1989. A new model for determining mean structure parameters of fixed beds from pressure drop measurements: application to beds packed with parallelepipedal particles. Chem. Eng. Sci. 44 (7), 1539–1545.
Dawson, M., 2009. Composite plates with a layer of fluid-filled, reticulated foam for blast protection of infrastructure. Int. J. Impact Eng. 36 (10), 1288–1295.
Dawson, M., McKinley, G., Gibson, L., 2008. The dynamic compressive response of open-cell foam impregnated with a newtonian fluid. J. Appl. Mech. 75 (4), 041015.
Dawson, M., McKinley, G., Gibson, L., 2009. The dynamic compressive response of an open-cell foam impregnated with a non-newtonian fluid. J. Appl. Mech. 76 (6), 061011.
Dvorkin, J., Nur, A., 1993. Dynamic poroelasticity: a unified model with the squirt and the biot mechanisms. Geophysics 58 (4), 524–533.
Fratzl, P., Kolednik, O., Fischer, F.D., Dean, M.N., 2016. The mechanics of tessellations–bioinspired strategies for fracture resistance. Chem. Soc. Rev. 45 (2), 252–267.
Gent, A.N., 2012. Engineering With Rubber: How to Design Rubber Components. Carl Hanser Verlag gmbh co KG.

Graesser, E., Wong, C., 1991. The Relationship of Traditional Damping Measures for Materials With High Damping Capacity.
Gurevich, B., Makarynska, D., de Paula, O.B., Pervukhina, M., 2010. A simple model for squirt-flow dispersion and attenuation in fluid-saturated granular rocks. Geophysics 75 (6), N109–N120.
Lakes, R.S., 1998. Viscoelastic Solids. vol. 9. CRC press.
Müller, T.M., Gurevich, B., Lebedev, M., 2010. Seismic wave attenuation and dispersion resulting from wave-induced flow in porous rocksa review. Geophysics 75 (5). 75A147–75A164.
Ogden, R.W., 1997. Non-linear Elastic Deformations. Courier Corporation.
Pride, S.R., Berryman, J.G., 2003. Linear dynamics of double-porosity dual-permeability materials. i. governing equations and acoustic attenuation. Phys. Rev. E 68 (3), 036603.
Quintal, B., Steeb, H., Frehner, M., Schmalholz, S.M., 2011. Quasi-static finite element modeling of seismic attenuation and dispersion due to wave-induced fluid flow in poroelastic media. J. Geophysical Res. 116 (B1).
Renner, J., Steeb, H., 2014. Modeling of fluid transport in geothermal research. In: Handbook of Geomathematics, pp. 1443–1500.
Rubino, J.G., Ravazzoli, C.L., Santos, J.E., 2008. Equivalent viscoelastic solids for heterogeneous fluid-saturated porous rocks. Geophysics 74 (1), N1–N13.
Schraad, M., Harlow, F., 2006. A multi-field approach to modeling the dynamic response of cellular materials. Int. J. Mech. Sci. 48 (1), 85–106.
Vinci, C., Renner, J., Steeb, H., 2014. On attenuation of seismic waves associated with flow in fractures. Geophysical Res. Lett. 41 (21), 7515–7523.
Zhang, D., Weinbaum, S., Cowin, S., 1998. Estimates of the peak pressures in bone pore water. J. Biomech. Eng. 120 (6), 697–703.